

Analysis of COVID-19 evolution in Senegal: impact of health care capacity

Mouhamed M. Fall, Babacar M. Ndiaye, Ousmane Seydi and Diaraf Seck

Abstract. We consider a compartmental model from which we incorporate a time-dependent health care capacity having a logistic growth. This allows us to take into account the Senegalese authorities response in anticipating the growing number of infected cases. We highlight the importance of anticipation and timing to avoid overwhelming that could impact considerably the treatment of patients and the well-being of health care workers. A condition, depending on the health care capacity and the flux of new hospitalized individuals, to avoid possible overwhelming is provided. We also use machine learning approach to project forward the cumulative number of cases from March 02, 2020, until 1st December, 2020.

Keywords. COVID-19, health care capacity, parameter estimates, logistic growth, forecasting, machine learning.

1. Introduction

COVID-19, declared a pandemic by the World Health Organization (WHO) [25] on 11 March 2020, is still spreading around the world up to date 26 September 2020. The number of people infected is beyond 32 million on 26 September 2020 with 989,380 deaths [24]. In Senegal, the number of cumulative cases is currently 14839 with 2624 individuals undergoing treatment on 25 September 2020[13]. The first cases, from Wuhan, were notified to WHO on 31 December 2019 [25, 26] while, Senegal notified its first case on 02 March 2020 [13]. Because of its limited resources, as in many sub-Saharan African countries, it is therefore valuable to understand the growth and the timing in responding to the logistic needs of their health system. We note that several developed countries that nevertheless have high-capacity health structures have been overwhelmed and this considerably impacted negatively in the combat against the pandemic. In [14] it is discovered that the growing number of COVID-19 cases in the United States could gravely challenge the critical care capacity, thereby exacerbating case fatality rates. As pointed out in [23], under-resourced health systems may pose a threat to patient care as well as the safety and well-being of health care workers.

From the appearance of the first cases of COVID-19, the Senegalese authorities decided to

anticipate by increasing gradually the capacity of its hospitals to take care of patients suffering from COVID-19. One of the aims of the present paper is to study different scenarios of involution of the number of virus patients by varying the growth rate and the number of, say, beds or rooms. As an approach, we use a mathematical model that integrates the different stages of individuals (Susceptible, Exposed, Asymptomatic, Symptomatic, Removed) with the parameters depending on the health resources availability. To this cope, we consider a modified SEWIR model [16] in which we include a time-dependent carrying capacity $K(t)$ representing the evolution of the Senegalese hospitals' capacity in response to the growing number of cases in Senegal. Our analysis highlights the importance of anticipation and timing to avoid overwhelming in the health system. More precisely, our analysis shows, in particular, that, while the epidemic grows exponentially fast, by respecting a certain logistic growth (at which the number of beds is being added) in the health system, the epidemic might remain under control. As a consequence, a non-negligible number of expenses can be saved.

Finally, a machine learning approach to project forward the cumulative number of virus infected cases is provided. Let us mention that several studies have been conducted in different contexts to assess the impact of hospital saturation in COVID-19. We refer for examples to [5, 7, 8, 14, 21] and the references therein. Our work complements several studies that have been carried out on the spread of Sars-CoV-2 in Senegal [2, 3, 4, 6, 15, 16, 17, 18]. It should be noted that the aforementioned studies did not address the impact of saturation on patients care in Senegal. However, some studies on the prediction of the number of new cases for Senegal have already been carried out using machine learning [2, 3, 15, 16] and on the impact of contaminated objects using compartmental models [6].

The paper is organized as follows. In section 2, we describe in detail our model as well as the parameters involved. It is followed by Section 3 concerning the estimation of the unknown parameters. In section 4 we derive the time-dependent effective reproduction number which is a key function that informs about the impact of the various decisions taken by the authorities during the epidemic. In Section 5, we first present the calibration of the model to the cumulative number of reported cases. We then present numerical simulations on the impact of the dynamics of health capacity on the patients care. Finally, in Section 6, we use machine learning to project forward the number of cumulative cases until 1st December 2020.

2. Model description

We consider compartmental epidemic model that incorporates a time-dependent carrying capacity $K(t)$ of health structures for the treatment of COVID-19 patients at the hospitals. The model reads as follow

$$\begin{cases} S'(t) &= -\beta_1(t)[W(t) + \varepsilon I(t)]S(t) \\ E'(t) &= \beta_1(t)[W(t) + \varepsilon I(t)]S(t) - \beta_2 E(t) \\ W'(t) &= \beta_2 E(t) - \beta_3 W(t) \\ I'(t) &= (1 - \alpha_1)\beta_3 W(t) - \gamma I(t) (1 - I(t)/K(t))_+ - \eta I(t) \\ R'(t) &= \alpha_1 \beta_3 W(t) + \gamma I(t) (1 - I(t)/K(t))_+ + \eta I(t) \end{cases} \quad (2.1)$$

with initial conditions

$$S(t_0) = S_0, E(t_0) = E_0, W(t_0) = W_0, I(t_0) = I_0, R(t_0) = R_0 \quad (2.2)$$

and

$$(1 - I(t)/K(t))_+ = \begin{cases} 1 - I(t)/K(t) & \text{if } I(t) \leq K(t) \\ 0 & \text{if } I(t) > K(t). \end{cases} \quad (2.3)$$

The state variable $S(t)$ is the number of susceptible individuals at time t , $E(t)$ the number of exposed individuals at time t and $W(t)$ the number of waiting cases for confirmation (with infectiousness) at time t . The number of confirmed and monitored cases at time t is denoted by $I(t)$. The variable $K(t)$ describes the effective carrying capacity of the health structure, which is the maximum number of $I(t)$ individuals that can be correctly monitored. Finally $R(t)$ represents the removed individuals at time t due to death or recovery. The figure below represents the diagram flux of the model. The term $\varepsilon\beta_1(t)I(t)S(t)$ represents the transmission of the disease within the health

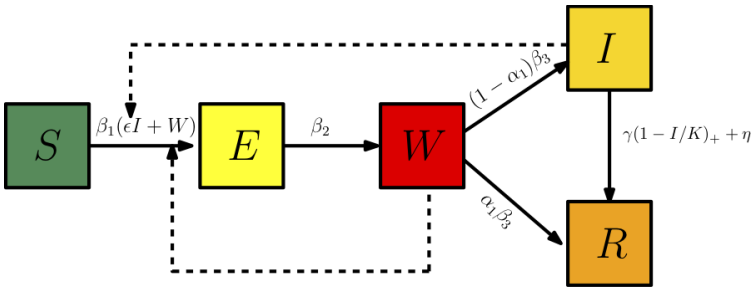


FIGURE 1. Flow diagram of the model.

structures where $\varepsilon > 0$ can be interpreted as the probability that a susceptible individual is working in the health system. More precisely we set $\varepsilon = N_H/S_0$ with N_H the number of health care workers and S_0 the initial number of susceptible individuals. The quantity of $1/\beta_2$ is the average incubation period. We assume that the average waiting time for confirmation is $1/\beta_3$ days. After the waiting time, a fraction $1 - \alpha_1$ is monitored while the remaining fraction α_1 is removed due to death or recovered. The removal rate of the confirmed cases is described by $t \rightarrow \gamma(1 - I(t)/K(t))_+ + \eta$ in order to take into account the saturation effect of the public health structures. The term $\gamma(1 - I(t)/K(t))_+ + \eta$ which is a decreasing function of $I(t)$ describes the efficiency of the health structures. The maximal efficiency is $\gamma + \eta$ while the minimal efficiency η is reached when the number of confirmed cases becomes greater than the carrying capacity $K(t)$. In our modeling procedure, we have introduced a time-dependent carrying capacity which is motivated by the fact that in Senegal, the carrying capacity of the health structures was gradually increased in response to the increase in the number of infected individuals. The dynamics of the increase in the number of beds remains unknown because only announcements have been made. We chose a logistic equation to mimic the growth of the public health capacity to its saturation. Indeed, from the onset of the epidemic, the authorities announced a carrying capacity of 30 which gradually increased according to the number of cases. The maximum capacity of the structures remains unknown but in view of the announcements made, we assume that it is approximately 3000. The growth rate $r = 0.1$ of $t \rightarrow K(t)$ is chosen such that it increases from 30 on 02 March to approximately 3000 on 10 June

and that the number of hospitalized individuals is below the effective carrying capacity. There are other possibilities of choosing the growth rate r but the value $r = 0.1$ appears to give the best fit to the data. The figure below describes the evolution of $K(t)$ with respect to time and the evolution of the number of hospitalized individuals.

The evolution of the public health capacity and number of monitored are illustrated in Figure 2.

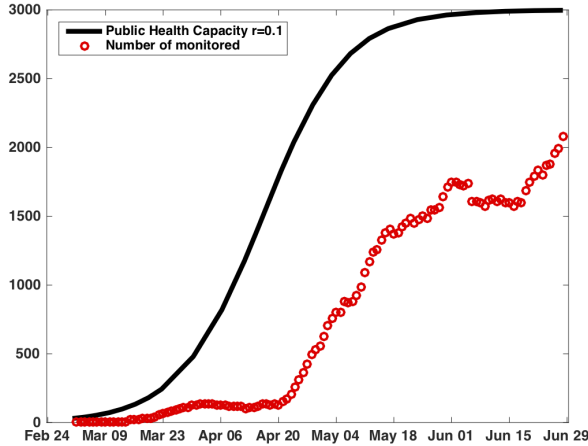


FIGURE 2. Evolution of the hospital carrying capacity and the number of hospitalized individuals.

More precisely the dynamic of the carrying capacity is given by:

$$\frac{dK}{dt} = \begin{cases} rK(1 - K/K_{max}) & \text{if } K \leq K_{sa} \\ 0 & \text{if } K > K_{sa} \end{cases} \quad (2.4)$$

with

$$K_0 = 30, \quad r = 0.1 \quad \text{and} \quad K_{max} = 3000.$$

The parameter K_{sa} will serve to explore different scenarios in which the efforts of increasing health capacities are aborted. In model (2.1)-(2.4), we use a time-dependent transmission rate to take into account the various events that have impacted the spread of disease. Indeed several government actions such as partial lockdown, social distancing, interurban traffic ban, border closure have impacted the progression of the disease. The time-dependent transmission rate has the following form

$$\beta_1(t) = \begin{cases} \beta_{10} & \text{if } t_0 \leq t < t_1 \\ \max(\beta_{10}e^{-\theta_1(t-t_1)}, \theta_2\beta_{10}) & \text{if } t_1 \leq t < t_2 \\ \min(\beta_{11}e^{\theta_1(t-t_2)}, \theta_3\beta_{10}) & \text{if } t_2 \leq t < t_3 \\ \max(\beta_{12}e^{-\theta_1(t-t_3)}, \theta_4\beta_{10}) & \text{if } t \geq t_3, \end{cases} \quad (2.5)$$

where the parameters are estimated by using the data on reported cases. More precisely we have

$$\beta_{11} = \max(\beta_{10}e^{-\theta_1(t_2-t_1)}, \theta_2\beta_{10}) \quad \text{and} \quad \beta_{12} = \min(\beta_{11}e^{\theta_1(t_3-t_2)}, \theta_3\beta_{10})$$

with $t_0 = 02$ March the date at which the first case was reported [13], $t_1 = 24$ March, $t_2 = 12$ April and $t_3 = 20$ April. We distinguish three phases. Phase 1 takes place between the dates $t_0 = 02$ March, the beginning of the epidemic, until the first government actions at date $t_1 = 24$ March. Phase 2 which begins at t_1 , the date on which decisions such as public closing, interurban traffic ban, border closure were taken, is ended at date $t_2 = 12$ April. The date t_2 corresponds to a sudden increase in the number of cases with a decline on approximately date $t_3 = 20$ April where Phase 3 began and cover the period of 20 April to 28 June the date at which we stop our study. The cause of the sudden increase in 12 April remains unknown to us at this time. More accurate data would be needed in order to understand the advent of this phenomenon. However, we can follow the evolution of the dynamics of the epidemic using the time-dependent transmission rate. The parameter θ_1 describes the intensity of the government actions or sudden events that impacted the transmission rate. We refer to [10] where such interpretation has been used to describes the government actions. The parameters θ_2 , θ_3 and θ_4 allow us to measure the impact of each phase on the transmission rate β_{10} . The values of the parameters θ_i , $i = 1, 2, 3, 4$ estimated in Section 3 are

$$\theta_1 = 5.1366, \theta_2 = 0.1224, \theta_3 = 1.7130, \theta_4 = 0.356, \tag{2.6}$$

and the estimated value of β_{10} in Section 3 is

$$\beta_{10} = 3.8593 \times 10^{-8}. \tag{2.7}$$

The figure below describes the transmission rate $t \rightarrow \beta_1(t)$. Next we summarize the

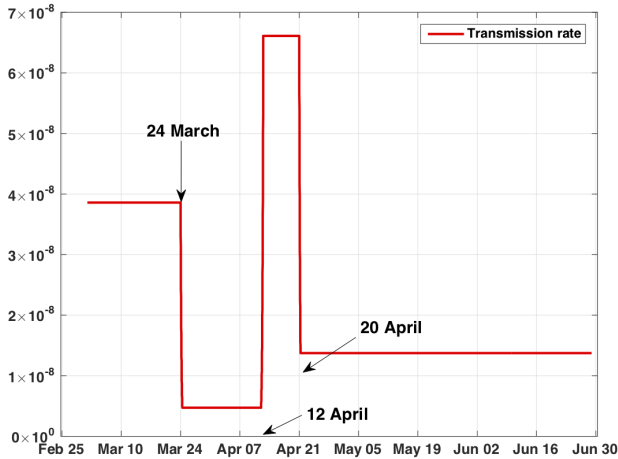


FIGURE 3. Time-dependent transmission $t \rightarrow \beta_1(t)$ of the period from 02 March to 28 June 2020.

descriptions of the remaining symbols in the table below. The values of fixed parameters in Table 1 are given in the next table

Symbol	Description	Method
t_0	Onset of the epidemic	fixed
S_0	Number of susceptible at time t_0	fixed
E_0	Number of exposed individuals at time t_0	fitted
W_0	Number of wating individuals at time t_0	fitted
I_0	Number of monitored infectious at time t_0	fitted
$\beta_1(t)$	Transmission rate	fitted
$1/\beta_2$	average latent period	fixed
β_3	Removal rate of the wating individuals	fixed
$1 - \alpha_1$	Fraction of wating individuals that become monitored	fitted
η	Rate at which monitored individuals are removed at hospital saturation	fixed
$\gamma + \eta$	Maximal removal rate of the monitored individuals	fixed
K_{max}	Maximal hospital carrying capacity	fixed
r	Intrinsic growth rate of the hospital carrying capacity	fixed
ε	Number of healthcare worker per susceptible individual	fixed

TABLE 1. Parameters of the model.

Symbol	Value	Reference
t_0	02 March 2020	[13]
S_0	7857353	[1]
$1/\beta_2$	1 day	[11]
$1/\beta_3$	10 days	WHO
α_1	30 %	Assumed
$1/\eta$	30 days	Assumed
$1/(\gamma + \eta)$	15 days	Assumed
K_{max}	3000	Assumed
K_0	30	Assumed
r	0.1	Assumed
ε	$1000/S_0$	Assumed

TABLE 2. Values of the fixed parameters.

3. Parameter estimates using the early phase

In this section, will use the approach developed in [9, 10, 11, 12] in order to estimate the parameters from the early phase of the epidemic. Let $C(t)$ be the cumulative number of reported cases at time t be defined by

$$C(t) = C(t_0) + (1 - \alpha_1)\beta_3 \int_{t_0}^t W(s)ds \quad (3.1)$$

with $t_0 = 02$ Mars 2020 the date of the first reported cases in Senegal so that $C(t_0) = 1$. The early phase of the epidemic corresponds to the period from the announcement of the first case on 02 Mars 2020 to the first government actions at $t_1 = 24$ March 2020.

In this phase we assume that the number of infected individuals growth exponentially. Hence with such assumption, the cumulative number of cases has the following form

$$C(t) = C(t_0) + \chi_2 e^{\chi_1(t-t_0)} - \chi_2, \quad t \in [t_0, t_1]. \quad (3.2)$$

The Figure 4 below shows the comparison between the $t \rightarrow C(t)$ and the data from 02 March until 24 March 2020 that allows us to estimate the parameters χ_1 and χ_2 to

$$\chi_1 = 0.1612 \quad \text{and} \quad \chi_2 = 1.979. \quad (3.3)$$

Assuming that $S(t)$ is approximately equal to $S(t_0)$ in the short time interval $[t_0, t_1]$ and

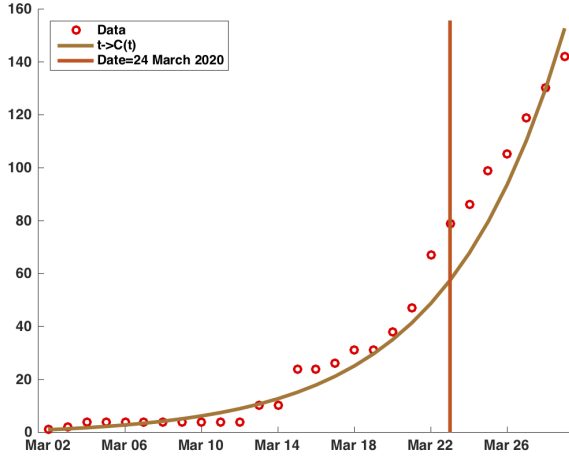


FIGURE 4. Comparison between the cumulative number of reported cases (data) and the map $t \rightarrow C(t)$ defined in (3.2).

that for each $t \in [t_0, t_1]$

$$E(t) = E_0 e^{\chi_1(t-t_0)}, \quad W(t) = W_0 e^{\chi_1(t-t_0)}, \quad I(t) = I_0 e^{\chi_1(t-t_0)}$$

and

$$\beta_1(t) = \beta_{10},$$

it follows that we have the following approximation for a short time period

$$\begin{cases} \chi_1 E_0 &= \beta_{10} S_0 (W_0 + \varepsilon I_0) - \beta_2 E_0 \\ \chi_1 W_0 &= \beta_2 E_0 - \beta_3 W_0 \\ \chi_1 I_0 &= (1 - \alpha_1) \beta_3 W_0 - (\gamma + \eta) I_0. \end{cases} \quad (3.4)$$

Furthermore differentiating (3.1) and (3.2) with respect to t we obtain

$$C'(t) = \chi_1 \chi_2 e^{\chi_1(t-t_0)} = (1 - \alpha_1) \beta_3 W(t) = (1 - \alpha_1) \beta_3 W_0 e^{\chi_1(t-t_0)}$$

that is

$$W_0 = \frac{\chi_1 \chi_2}{(1 - \alpha_1) \beta_3}. \quad (3.5)$$

Solving the second and the third equation of (3.4) we get:

$$E_0 = \frac{\chi_1 + \beta_3}{\beta_2} W_0 \quad \text{and} \quad I_0 = \frac{(1 - \alpha_1) \beta_3}{\chi_1 + \gamma + \eta} W_0. \quad (3.6)$$

Plugging (3.5) and (3.6) into the first equation of (3.4), it follows that

$$\beta_{10} = \frac{\chi_1 + \beta_2}{S_0(W_0 + \varepsilon I_0)} E_0. \quad (3.7)$$

Therefore using (3.3) together with (3.5)-(3.7) and the values of the parameters of Table 1 we obtain

$$E_0 = 1.18, \quad W_0 = 4.55, \quad I_0 = 1.39 \quad (3.8)$$

and

$$\beta_{10} = 3.8593 \times 10^{-8}. \quad (3.9)$$

In order to obtain the values of the parameters θ_i , $i = 1, 2, 3, 4$ that appear in the transmission rate $t \rightarrow \beta_1(t)$ we perform a curve fitting by using the data from $t_1 = 23$ March 2020 until 28 June 2020. The estimated values are listed below

$$\theta_1 = 5.1366, \quad \theta_2 = 0.1224, \quad \theta_3 = 1.7130, \quad \text{and} \quad \theta_4 = 0.356.$$

4. The effective reproduction number

The effective reproduction number, \mathcal{R}_e , is the expected number of secondary cases produced by one typical infection joining a healthy population during its infectious period while the time-dependent effective reproduction number $\mathcal{R}_e(t)$ is the instantaneous transmissibility of the disease at time t . The time-dependent effective reproduction number allows to follow the evolution of the epidemic as the time evolves in particular how $\mathcal{R}_e(t)$ is far above or far below 1.

In order to obtain $\mathcal{R}_e(t)$ we note that $\beta_1(t)S(t)$ is the number of new infections per unit of time generated by one infectious individual. Thus assuming $\beta_1(t)S(t)$ approximately constant during $1/\beta_3$, it follows that the term

$$\frac{\beta_1(t)S(t)}{\beta_3}$$

is the average number of new infections generated by one infectious individual (W) during its period of infectiousness $1/\beta_3$. Moreover one infectious individual (W) generates on average

$$(1 - \alpha_1)\beta_3 \times 1 \times \frac{1}{\beta_3} = 1 - \alpha_1$$

infectious individual(s) (I). Those $1 - \alpha_1$ infectious (I) has a maximum mean infectiousness period $1/(\gamma + \eta)$ so that they generate

$$\varepsilon\beta_1(t)S(t) \times (1 - \alpha_1) \times \frac{1}{\gamma + \eta}$$

new infections after $\frac{1}{\gamma + \eta}$ times.

We finally define the time-dependent effective reproduction number as

$$\mathcal{R}_e(t) = \frac{\beta_1(t)S(t)}{\beta_3} + \frac{(1 - \alpha_1)\varepsilon\beta_1(t)S(t)}{\gamma + \eta}. \quad (4.1)$$

The figure below gives the evolution of the effective reproduction number. We observe that the effective reproduction number is larger than 1 (approximately 3) during the early phase of the epidemic that is from 02 March to 24 March and is smaller than 1 during the second Phase. We can therefore observe that the first actions of the government had a

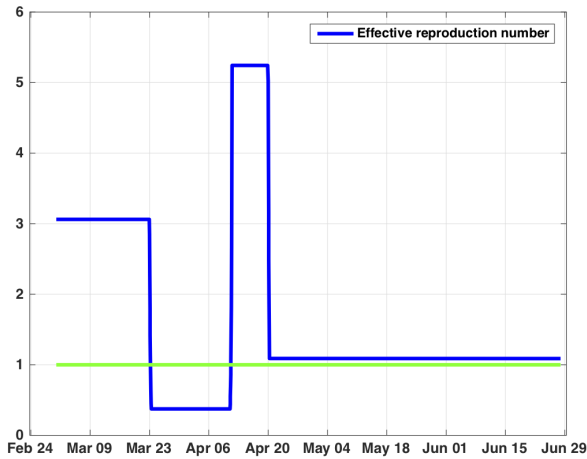


FIGURE 5. The effective reproduction $t \rightarrow \mathcal{R}_e(t)$ of the period from 02 March to 28 June 2020.

positive effect on the spread of the epidemic because it tended to disappear if the effective measures would have been kept in the same trend. However, the sudden increase in cases on April 12th impacted the effective reproduction number to bring it to around 5. It goes down until it is close to but greater than 1 from April 20th. The cause of this increase is unknown to us but a better knowledge of the data may allow us to find an explanation.

5. Numerical simulations

In this section we perform numerical simulations of the dynamics of the spread of the COVID-19 epidemic based on our proposed model (2.1)-(2.4). We consider the regions of Dakar, Thies and Diourbel which concentrate around 95% of the reported cases. To do so we assume that the initial number of susceptibles is the population of Dakar, Thies and Diourbel, that is to say $S_0 = 7857353$ [1]. The values of the parameters of the model are listed in Table 2. The time-dependent transmission rate is given in (2.5)-(2.7) while the estimated initial conditions in Section 3 are $E_0 = 1.18$, $W_0 = 4.55$, $I_0 = 1.39$. In Figure 6 below we compare the cumulative number of cases $t \rightarrow C(t)$ defined in (3.1) with 95% of the cumulative number of reported cases showing that our model agrees with the data. In order to illustrate the impact of the saturation of health structures on the number of monitored individuals, we consider several scenarios. Indeed, we consider the same evolution of the reception capacity with interruptions in growth at predefined values. More precisely we consider the following dynamic

$$\frac{dK}{dt} = \begin{cases} rK(1 - K/K_{max}) & \text{if } K \leq K_{sa} \\ 0 & \text{if } K > K_{sa} \end{cases} \quad (5.1)$$

where K_{sa} , the saturation level, is respectively 3000, 2500, 2000, 1500 and 1000 and is illustrated by the following figure. In Figure 8 we plot the corresponding number of monitored individuals that is $t \rightarrow I(t)$ when the dynamics of the carrying capacity is given by (5.1) with $K_{sa} = 3000, 2500, 2000, 1500$ and 1000 while the growth rate is fixed at $r = 0.1$. We see that the epidemic is under control, until 28 June only when $K_{sa} = 3000$

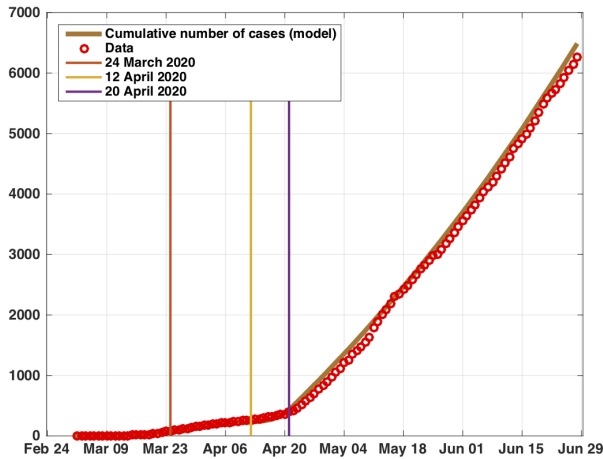


FIGURE 6. Comparison between 95 % of the cumulative number of reported cases to the model for the population of Dakar, Thies and Diourbel.

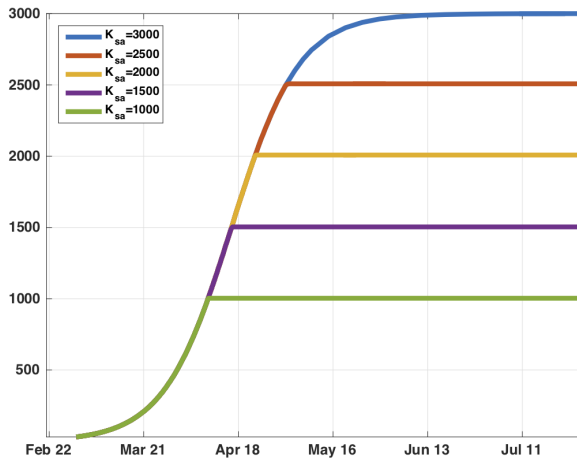
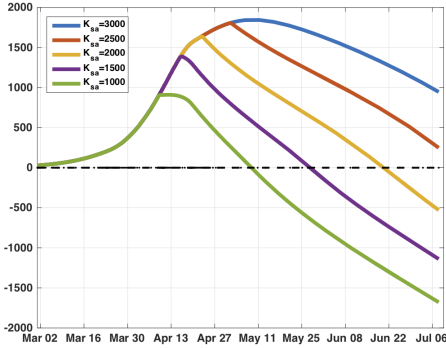


FIGURE 7. Evolution of the carrying capacity with saturation at $K_{sa} = 3000, 2500, 2000, 1500$ and 1000 .

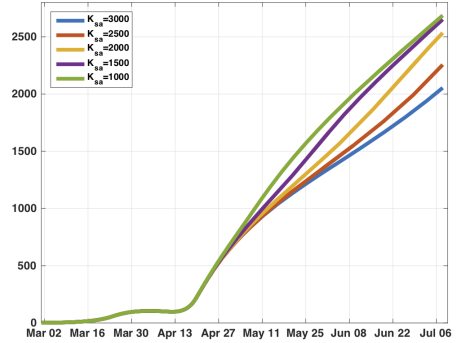
and $K_{sa} = 2500$. This shows that the maximum value of the carrying capacity, K_{sa} , may impact significantly the efficiency of public health structures by slowing down the rate at which individuals are removed from the hospital. In Figure 9 we look at the influence of the growth rate r on the number of monitored individuals. We see that increasing r from 0.1 to 0.5, does not impact significantly the number of monitored individuals and the dates at which overwhelming occurs. This is the case for all values of K_{sa} .

For $r = 0.05$, Figure 10, we see that the number of monitored individuals becomes larger than the maximum number of available resources at the early stage of the epidemic, around 20 April. We also observe that $I(t)$ remains unchanged for different values of K_{sa} . Thus our model captures and validates the obvious fact that the faster you increase the

number of beds, the better you can handle the hospitalized people. Figure 10 emphasizes more the sensibility of the growth rate r which can also be seen/interpreted as the timing in anticipating overwhelming. Indeed we observe that for the maximal value of resources $K_{sa} = K_{max} = 3000$, $K(t)$ stay larger than $I(t)$ until 28 June for $r \geq 0.06$ while for $r \leq 0.05$ we see that the number monitored becomes larger than available resources from mid-April to the end of June.

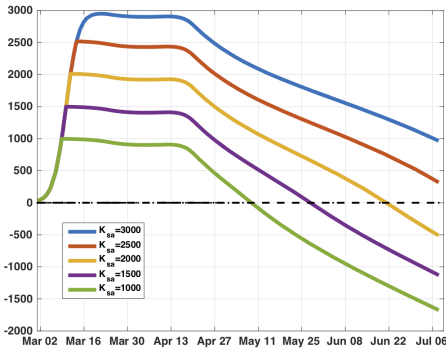


(A)

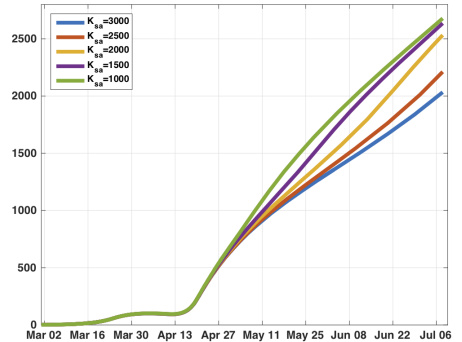


(B)

FIGURE 8. Number of monitored individuals with respect to the saturation carrying capacities values $K_{sa} = 3000, 2500, 2000, 1500$ and 1000 . The growth rate is $r = 0.1$. Figure (A) shows the difference $K(t) - I(t)$ and Figure (B) shows the evolution of monitored individuals $I(t)$.



(A)



(B)

FIGURE 9. Number of monitored individuals with respect to the saturation carrying capacities values $K_{sa} = 3000, 2500, 2000, 1500$ and 1000 . The growth rate is $r = 0.5$. Figure (A) shows the difference $K(t) - I(t)$ and Figure (B) shows the evolution of monitored individuals $I(t)$.

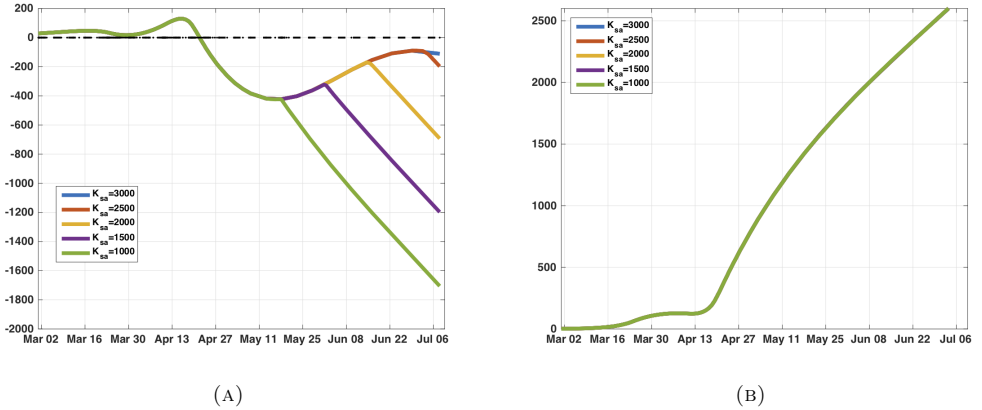


FIGURE 10. Number of monitored individuals with carrying capacities values $K_{sa} = 3000, 2500, 2000, 1500$ and 1000 . The growth rate is $r = 0.05$. Figure (A) shows the difference $K(t) - I(t)$ and Figure (B) shows the evolution of the monitored individuals $I(t)$.

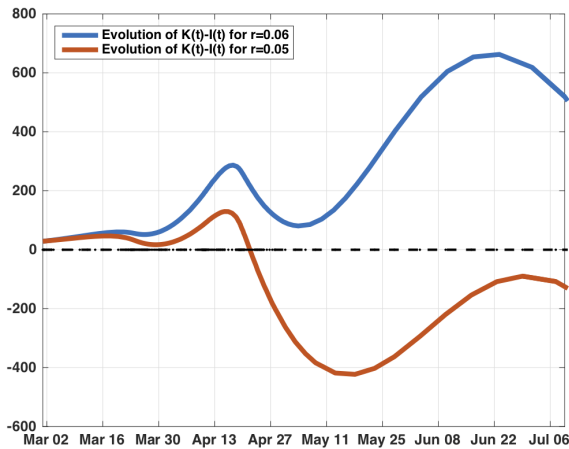


FIGURE 11. Number of monitored individuals with carrying capacity values $K_{sa} = 3000$. The growth rates are $r = 0.05$ and $r = 0.06$.

In view of our discussion, it would be important to have a condition that guarantees the unsaturation of health structures. It is contained in the following

Lemma 5.1. *Assume that $K_0 > I_0$. Assume in addition that $t \rightarrow K(t)$ is increasing and differentiable with respect to t . If*

$$\frac{(1 - \alpha_1)\beta_3 W(t)}{\eta} < K(t), \quad \forall t \in [t_0, T] \tag{5.2}$$

for some $T > 0$ then we have

$$I(t) < K(t), \forall t \in [t_0, T].$$

Proof. Define

$$J(t) := K(t) - I(t), \forall t \geq t_0.$$

Then, by assumption $J(t_0) = K_0 - I_0 > 0$ and by continuity there is $t_1 > t_0$ such that $J(t) > 0$ for each $t \in [t_0, t_1]$. Define

$$\bar{t} := \sup \{t_0 < t \leq T : J(s) > 0, \forall s \in [t_0, t]\}.$$

Next, we show that $\bar{t} \geq T$. Assume by contradiction that $\bar{t} < T$. Then we have $J(\bar{t}) = 0$ that is $I(\bar{t}) = K(\bar{t})$ so that by (5.2)

$$J'(\bar{t}) = K'(\bar{t}) - I'(\bar{t}) \geq \eta I(\bar{t}) - (1 - \alpha_1)\beta_3 W(\bar{t}) = \eta K(\bar{t}) - (1 - \alpha_1)\beta_3 W(\bar{t}) > 0.$$

This means that J is locally strictly increasing from \bar{t} which contradict the definition of \bar{t} . \square

Remark 5.2. Let us note that condition (5.2) can be used in practice. Indeed $1/\eta$ is known and $(1 - \alpha_1)\beta_3 W(t)$ is the flux of new monitored individuals which is bounded above by the daily number of COVID-19 positive tests. Since $K(t)$ is a controllable quantity, the condition (5.2) may serve to anticipate an overwhelming over time.

It is important to note that in the above Lemma, we do not require $K(t)$ to have logistic growth. We only require $K(t)$ to be an increasing function.

6. Machine learning for forecasting

In this section, we present a machine learning approach for the forecasting of the cumulative number of confirmed cases $C(t)$. First, we collect the pandemic data from [13], from March 02, 2020, to October 22, 2020. Then, we perform a forecast with Prophet to predict the final size of coronavirus epidemic

The numerical tests are performed by using Python with the Panda library [20], and were executed on a computer with the following characteristics: intel(R) Core-i7 CPU 2.60GHz, 24.0Gb of RAM, under the UNIX system.

6.1. Prophet model

Prophet [19, 22], is a procedure for forecasting time series data based on an additive model where non-linear trends are fit with yearly, weekly, and daily seasonality, plus holiday effects. It works best with time series that have strong seasonal effects and several seasons of historical data. Prophet is robust in dealing with missing data and shifts in the trend and typically handles well outliers. For the averaging method, the forecasts of all future values are equal to the average (or “mean”) of the historical data. If we let the historical data be denoted by y_1, \dots, y_T , then we can write the forecasts as

$$\hat{y}_{T+h|T} = \bar{y} = (y_1 + y_2 + \dots + y_T)/T$$

The notation $\hat{y}_{T+h|T}$ is a short-hand for the estimate of y_{T+h} based on the data y_1, \dots, y_T . A forecasting interval gives an interval within which we expect y_t to lie on, with a specified probability. For example, assuming that the forecast errors are normally distributed, a 95% forecasting interval for the h -step forecast is

$$\hat{y}_{T+h|T} \pm 1.96\hat{\sigma}_h$$

where σ_h is an estimate of the standard deviation of the h -step forecast distribution.

6.1.1. Diagnostics. Here, we make some diagnostics by using the cross validation (see Table 3) and the performance metrics (see Table 4) using mse, rmse, mae and mape. The Figure 15 illustrate these cross validation metrics, making 10 forecasts with cutoffs between 2020-10-08, 00:00:00 and 2020-10-17, 00:00:00 (initial='220 days', period='1 days', horizon = '5 days').

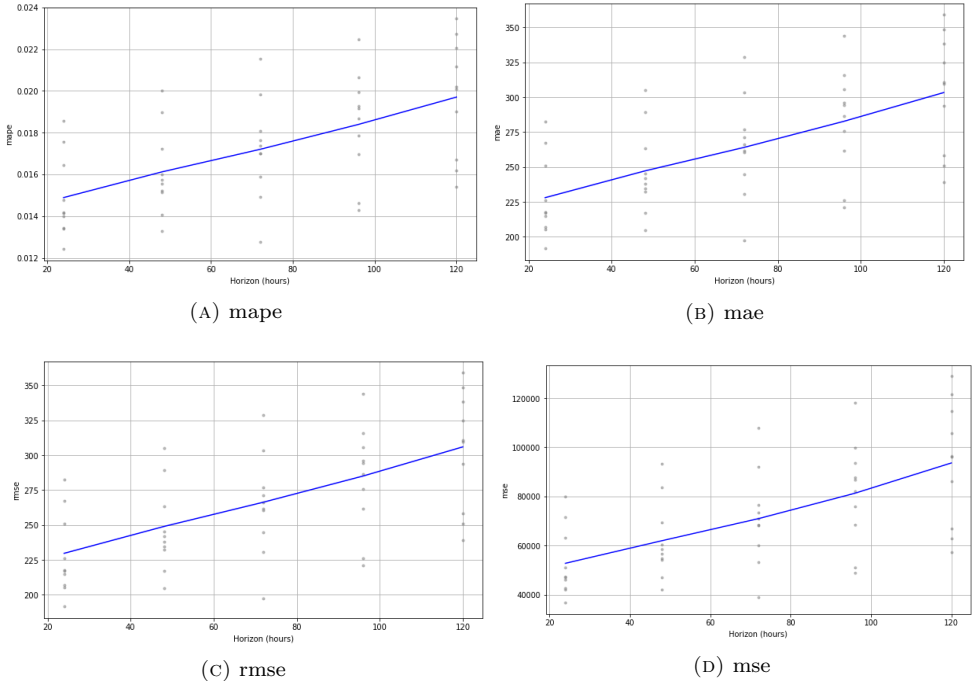


FIGURE 12. Senegal: cross validation metrics

ds	\hat{y}	\hat{y}_{lower}	\hat{y}_{upper}	y	cutoff
2020-10-09	15495.491181	15364.133271	15630.001589	15213	2020-10-08
2020-10-10	15549.266664	15412.256057	15684.595605	15244	2020-10-08
2020-10-11	15596.622824	15460.701411	15730.823401	15268	2020-10-08
2020-10-12	15635.801860	15501.234167	15775.220030	15292	2020-10-08
2020-10-13	15666.025418	15524.679008	15804.770389	15307	2020-10-08

TABLE 3. Senegal: cross validation

From Table 3, by comparing the values obtained on October 13, 2020 (column $y=15307$) with the predicted one (column $\hat{y}=15666.025418$), we see that the error is 2.29%. The predicted value is always within the confidence interval. So, Prophet seems to give us good value.

horizon	mse	rmse	mae	mape
1 days	52758.210719	229.691556	227.994396	0.014891
2 days	61956.779147	248.911187	247.169729	0.016120
3 days	70940.217291	266.346048	264.104073	0.017201
4 days	81284.637112	285.104607	282.785870	0.018392
5 days	93627.316861	305.985812	303.367943	0.019704

TABLE 4. Senegal: performance metrics

6.1.2. Trend changepoints and forecasting. The rmse for Prophet Model is 53.358002. The Prophet forecasting of confirmed cases, with trend changepoints, is given by Figure 13, and the trends and weekly increase are given by Figure 14. With Prophet, at \sim November 12, 2020 we may obtain > 16330 confirmed cases and > 16950 confirmed cases at \sim December 01, 2020 (see Tables 5 and 6, respectively). The forecastes of confirmed cases are illustrated in Figures 15a and 15b.

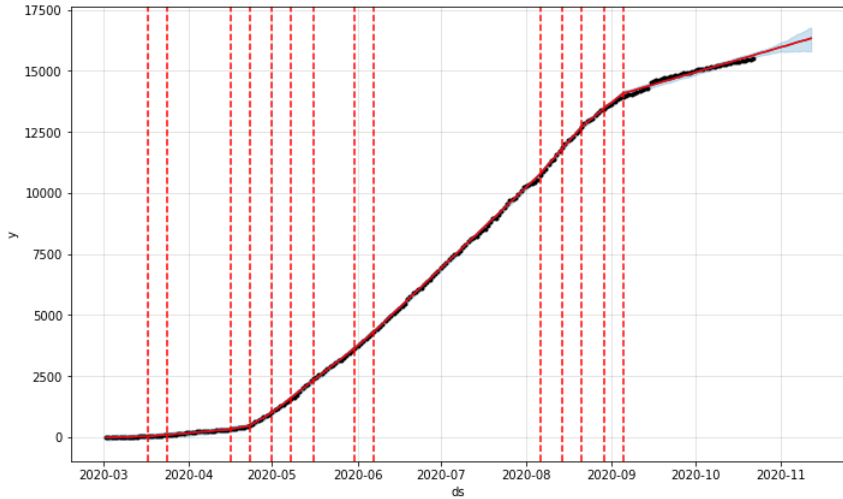


FIGURE 13. Senegal: changepoints of confirmed cases

ds	\hat{y}	\hat{y}_{lower}	\hat{y}_{upper}
2020-11-08	16213.793455	15776.476419	16625.216492
2020-11-09	16237.542798	15730.499926	16673.834380
2020-11-10	16254.670226	15734.183777	16750.503940
2020-11-11	16297.865380	15743.971264	16792.203760
2020-11-12	16335.788237	15755.096121	16875.197916

 TABLE 5. Prophet: predicted cumulative confirmed cases \sim November 12, 2020.

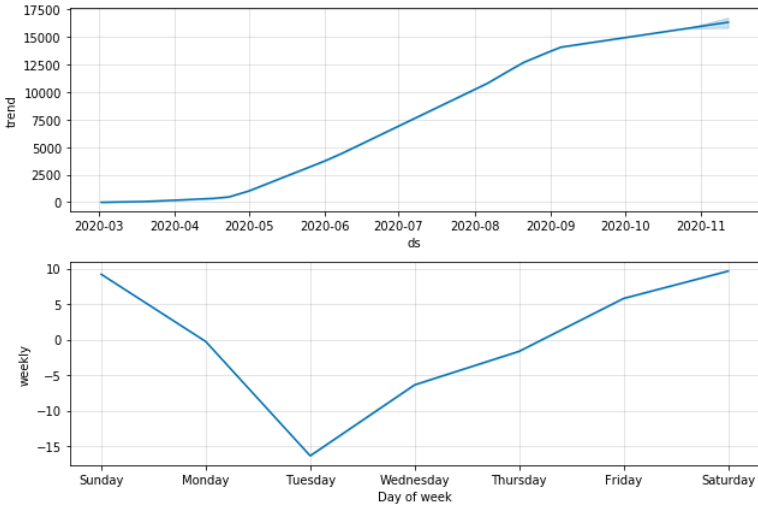
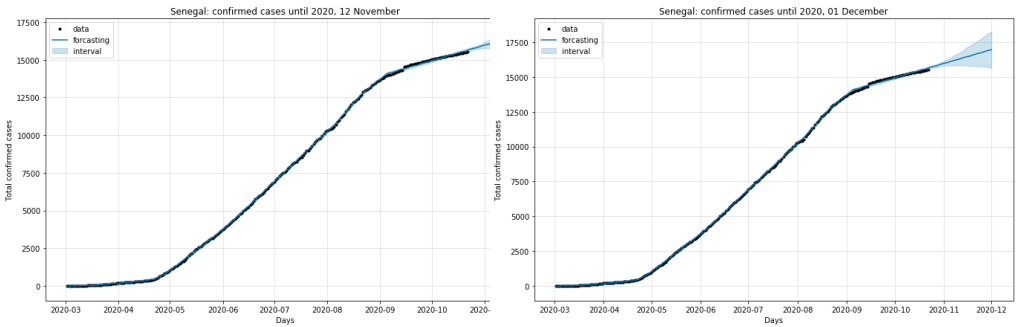


FIGURE 14. Senegal: Trends and weekly indrease of confirmed cases

ds	\hat{y}	\hat{y}_{lower}	\hat{y}_{upper}
2020-11-27	16841.363557	15724.240087	17997.233129
2020-11-28	16878.418793	15728.625383	18059.596350
2020-11-29	16911.177665	15665.479745	18162.293121
2020-11-30	16934.927009	15683.579005	18193.215306
2020-12-01	16952.054437	15654.901112	18268.706253

TABLE 6. Prophet: predicted cumulative confirmed cases ~December 01, 2020.



(A) 3 weeks forecasting

(B) 40 days forecasting

FIGURE 15. Senegal: Prophet for forecasting of confirmed cases

References

[1] Agence Nationale de la Statistique et de la Démographie (ANSD), Senegal. Available online: <https://www.ansd.sn> (accessed on 26 September 2020).

- [2] B.M. Ndiaye, M.A.M.T. Balde, D. Seck, Visualization and machine learning for forecasting of COVID-19 in Senegal, arXiv:2008.03135 [q-bio.PE], 6 Aug 2020, <https://arxiv.org/pdf/2008.03135>.
- [3] M.A.M.T. Balde, C. Balde, B.M. Ndiaye, Impact studies of nationwide measures COVID-19 anti-pandemic: compartmental model and machine learning, arXiv:2005.08395 [q-bio.PE], 17 May 2020, <https://arxiv.org/pdf/2005.08395>.
- [4] M.A.M.T. Balde, Fitting SIR model to COVID-19 pandemic data and comparative forecasting with machine learning, *medRxiv* (2020). <https://doi.org/10.1101/2020.04.26.20081042>.
- [5] J.J. Cavallo, D.A. Donoho, H.P. Forman, Hospital Capacity and Operations in the Coronavirus Disease 2019 (COVID-19) Pandemic—Planning for the Nth Patient, JAMA Health Forum, Published online March 17, 2020. doi:10.1001/jamahealthforum.2020.0345.
- [6] M. Diaby, O. Diop, A. Konté, and A. Sène, A. COVID-19 Propagation Mathematical Modeling: The Case of Senegal. Preprints 2020, 2020060224 doi:10.20944/preprints202006.0224.v1.
- [7] R. Djidjou-Demasse, Y. Michalakis, M. Choisy, M. T. Sofonea, S. Alizon, Optimal COVID-19 epidemic control until vaccine deployment, medRxiv (2020). doi:<https://doi.org/10.1101/2020.04.02.20049189>.
- [8] IHME COVID-19 health service utilization forecasting team, C. J.L. Murray, Forecasting COVID-19 impact on hospital bed-days, ICU-days, ventilator-days and deaths by US state in the next 4 months, medRxiv (2020). doi:<https://doi.org/10.1101/2020.03.27.20043752>.
- [9] Z. Liu, P. Magal, O. Seydi, G. F. Webb, Understanding unreported cases in the 2019-nCov epidemic outbreak in Wuhan, China, and the importance of major health interventions, *MPDI Biology* (2020), 9, 50.
- [10] Z. Liu, P. Magal, O. Seydi, G. F. Webb, Predicting the cumulative number of cases for the COVID-19 in China from early data, *Mathematical Biosciences and Engineering*, 17(4), (2020), 3040-3051.
- [11] Z. Liu, P. Magal, O. Seydi, G. F. Webb, A COVID-19 epidemic model with latency period, *Infectious Disease Modelling* 5 (2020), 323-337.
- [12] Z. Liu, P. Magal, O. Seydi, G. F. Webb, A model to predict COVID-19 epidemics with applications to South Korea, Italia, and Spain, *SIAM News*, 53(4) (2020).
- [13] Ministre de la santé et de l'action sociale. Situation du Covid-19 au Sénégal. Available online: www.sante.gouv.sn/ (accessed on 26 September 2020).
- [14] S. M. Moghadas, et al., Projecting hospital utilization during the COVID-19 outbreaks in the United States, *Proceedings of the National Academy of Sciences*, 117(16), (2020), 9122-9126.
- [15] B.M. Ndiaye, L. Tendeng, D. Seck, Analysis of the COVID-19 pandemic by SIR model and machine learning technics for forecasting, arXiv:2004.01574 [q-bio.PE], 3 Apr 2020, <https://arxiv.org/pdf/2004.01574>.
- [16] B.M. Ndiaye, L. Tendeng, D. Seck, Comparative prediction of confirmed cases with COVID-19 pandemic by machine learning, deterministic and stochastic SIR models, arXiv:2004.13489 [q-bio.PE], 24 Apr 2020, <https://arxiv.org/pdf/2004.13489>.
- [17] V.M. Ndiaye, S.O. Sarr, B.M. Ndiaye, Impact of contamination factors on the COVID-19 evolution in Senegal, arXiv:2006.16326 [q-bio.PE], 29 Jun 2020, <https://arxiv.org/pdf/2006.16326>.
- [18] M. Samb, B.M. Ndiaye, Logistic growth model and modeling of factors for community case transmission, arXiv:2011.02766 [q-bio.PE], 5 Nov 2020, <https://arxiv.org/pdf/2011.02766v1>.

- [19] Prophet: Automatic Forecasting Procedure. Available online: <https://facebook.github.io/prophet/docs/> or <https://github.com/facebook/prophet> (accessed on 26 September 2020).
- [20] Python Software Foundation. Python Language Reference, version 2.7. Available online: <http://www.python.org> (accessed on 26 September 2020).
- [21] Q. Richard, S. Alizon, M. Choisy, M. T. Sofonea, R. Djidjou-Demasse, Age-structured non-pharmaceutical interventions for optimal control of COVID-19 epidemic, medRxiv (2020). doi:<https://doi.org/10.1101/2020.06.23.20138099>.
- [22] S.J. Taylor, B. Letham, Forecasting at scale, PeerJ Preprints (2017) 5:e3190v2<https://doi.org/10.7287/peerj.preprints.3190v2>.
- [23] G. E. Weissman et al., Locally Informed Simulation to Predict Hospital Capacity Needs During the COVID-19 Pandemic, Annals of internal medicine, 173(1), (2020), 21-28.
- [24] Wikipedia, Template:COVID-19 pandemic data. Available online: https://en.wikipedia.org/wiki/Template:COVID-19_pandemic_data (accessed on 26 September 2020).
- [25] WHO Timeline–COVID-19. Available online: <https://www.who.int/news-room/detail/27-04-2020-who-timeline---covid-19> (accessed on 26 September 2020).
- [26] World Health Organization. Pneumonia of Unknown Cause–China.Disease Outbreak News, 5 January 2020. Available online: <https://www.who.int/csr/don/05-january-2020-pneumonia-of-unkown-cause-china/en/> (accessed on 26 September 2020).

Mouhamed M. Fall
 The African Institute for Mathematical Sciences (AIMS)
 Mbour, Senegal.
 e-mail: mouhamed.m.fall@aims-senegal.org

Babacar M. Ndiaye
 Laboratory of Mathematics of Decision and Numerical Analysis
 University of Cheikh Anta Diop.
 BP 45087, 10700. Dakar, Senegal.
 e-mail: babacarm.ndiaye@ucad.edu.sn

Ousmane Seydi
 Département Tronc Commun,
 École Polytechnique de Thiès, Senegal.
 e-mail: oseydi@ept.sn

Diaraf Seck
 Laboratory of Mathematics of Decision and Numerical Analysis
 University of Cheikh Anta Diop, Dakar, Senegal.
 IRD, UMMISCO, Dakar, Senegal.
 e-mail: diaraf.seck@ucad.edu.sn